A regenerative braking system for internal combustion engine vehicles based on supercapacitors - Part 1: System analysis and modelling

Emiliano Pipitone[a], Gianpaolo Vitale[b,*]

[a] Department of Engineering, University of Palermo, Italy

[b] ICAR, Institute for high performance computing and networking, National Research Council of Italy

[*] Corresponding author: gianpaolo.vitale@icar.cnr.it

Abstract: In this two-parts work an electric Kinetic Energy Recovery System (e-KERS) for internal combustion engine vehicle (ICEV) is presented and its performance evaluated through numerical simulations. The KERS proposed is based on the use of supercapacitors as energy storage, interfaced to a brushless machine through a properly designed power converter. In part 1 the system is described and analyzed, and the mathematical model used for the simulations is presented. For each component of the KERS, the real efficiency and the power or energy limitations are adequately considered. In part 2 the energetic and economic advantages attainable by the proposed KERS are evaluated using MATLAB Simulink, considering a widely diffused gasoline passenger car and two reference driving cycles (ECE-15 and Artemis Urban). Energy savings of the order of 16% were found, with a slight increase in vehicle weight (+2%) and with an overall commercial cost that would be compensated in 7 years thanks to the fuel economy improvement, to which corresponds an equal reduction of CO_2 emissions. The low complexity of the system, never proposed for ICEV, the moderate weight of its components and their availability on the market, make the solution presented ready for the introduction in current vehicle production.

Keywords: Kinetic Energy Recovery System; Supercapacitor; Ultracapacitor; Vehicle Fuel economy; Regenerative Braking; Urban Driving Cycle; Hybrid Vehicle;

1 Introduction

The growing demand for sustainable mobility is driving researchers and vehicles manufacturers towards the exploration of low fuel consumption and environmental friendly solutions. The ever growing attention to road transport emission and urban pollution [1], the advances in the combustion and control of alternative and cost effective fuels [2] [3], the optimal management of vehicles drive-lines [4] [5] as well as the energy management techniques applied to

electric vehicles (EV) [6][7][8][9] are only few examples of the strong technological effort towards a sustainable and emission free mobility. Nevertheless, one of the heaviest lack in the management of traditional internal combustion engines vehicles (ICEV) is the huge amount of energy lost during braking phases. The vehicle kinetic energy, if recovered and not dissipated as heat by traditional braking system, could be efficiently employed for successive vehicle acceleration phases or for general vehicle energy requirement, and could substantially contribute to lower the energy consumption of the vehicles and the pollution associated. Studies show that, in urban driving situations, conventional braking systems discard as heat to the atmosphere about one third to one half of the energy of the power plant [10].

Several Regenerative Braking Systems (RBS) or Kinetic Energy Recovery Systems (KERS) have been proposed in literature, studied and optimized for different kind of vehicles (Electric, Hybrid or Internal combustion engine vehicle), with energy storage system of different kind (mechanical, electrical, chemical, hydraulic), and suitable or not for retrofit application on current production vehicles.

Regenerative braking has been intensively studied and implemented on Hybrid Electric Vehicles (HEV), including Fuel Cell Hybrid Electric Vehicles and Plug-In Hybrid Electric Vehicles: in these vehicles, the presence of powerful electric machines (generator and motor) interfaced to high capacity energy storage (e.g. batteries[1]), easily allows to convert and store vehicle kinetic energy into electric energy, which is then employed for vehicle propulsion. Also pure Electric Vehicles (EV) may easily benefit from regenerative braking if equipped with a properly sized generator, i.e. a generator capable of managing the braking power.

Unlike electrified vehicles, internal combustion engine vehicles are not equipped with generator, motor and batteries of adequate power and capacity to allow the conversion of the vehicle kinetic energy into electric energy, as well as its storage and re-utilization for vehicle propulsion. For this reason, the kinetic energy recovery systems successfully tested for ICEV application are mainly based on mechanical and hydraulic energy storage devices. Spring and elastomers, for example, have been considered as KERS storage element, relying on the (mechanical) energy storable by deforming an elastomer or a metallic spring [11]: the main advantage is the efficiency of the system, since the conversion into electric energy is not required. Simulations revealed that a 15% potential fuel economy improvement can be achieved, but, besides a significant space to be fitted, the system also requires the use of a Continuous Variable Transmission (CVT), thus adding complexity and significant weight to the vehicle.

Another pure mechanical system is represented by flywheel KERS, which stores the vehicle kinetic energy into rotational energy of a flywheel. As reported in literature [11][12] flywheel KERS can recover up to 70% of vehicle

[1] Although a battery is an energy converter, it is usually referred to as an energy storage, which is the same terminology adopted in this paper

kinetic energy and produce fuel consumption reduction in the order of 20%. However, the energy recovered cannot be permanently stored, due to mechanical and fluid dynamics friction on the flywheel. For this reason, vacuum chamber and magnetic bearings must be employed to obtain the best results. Moreover, to fully exploit its potential, this kind of KERS requires the use of a CVT and of lightweight composite flywheel: as an overall result, besides the added weight (65 kg for a 1800 kg vehicle) these high-technology components substantially increase the cost and complexity of the system. Average values for power and energy storage of high tech flywheel KERS are around 60kW and 400 kJ respectively [12].

Pneumatic and hydraulic KERS have also been studied for internal combustion engine vehicles: in these cases energy is stored by increasing the pressure of a fluid, which can be air (pneumatic type [13]) or a non-compressible fluid (hydraulic type [11]); the energy is then released back to the powertrain by decreasing the pressure of the fluid. Simulations showed that the pneumatic KERS with 300 kJ of energy storage may achieve 20% fuel efficiency improvement, while vehicle efficiency improvement of 35% are expected with hydraulic system with energy storage of 90 kJ. However, the additional space and weight of the added tanks and accumulators (for a pneumatic type, a storage tank of 50 L is necessary for a 1-ton vehicle [13]) make this KERS more suitable for heavy vehicles, rather than for passenger cars. Moreover, the required modifications to the powertrain, which should be endowed of a CVT, make them unsuitable for retrofit.

The only kind of electric KERS currently studied and developed for internal combustion engine vehicles is represented by alternator-control KERS, which has been already introduced in the market by some car manufacturer (e.g. BMW Efficient Dynamics [14]): with this kind of systems, the alternator output is increased during braking phases thus transferring part of the vehicle kinetic energy to the battery, whose energy is employed to supply electrical consumers of the vehicle, thus reducing the power absorbed by the alternator during vehicle positive traction phases. The advantage of this system relies on its immediate applicability to current ICEV production, but, being realized with component not dedicated or optimized for KERS application, the fuel economy improvement is limited, ranging from 1% to 5% [11].

In the present paper the authors propose an electric Kinetic Energy Recovery System (e-KERS) for internal combustion engine vehicles composed of a supercapacitors bank (SC), used as electric energy storage system, a motor-generator unit (MGU) to convert vehicle kinetic energy into electric energy and vice versa, and a power converter (PC), whose task is to manage power transfer between SC and MGU: the system was conceived to recover the vehicle kinetic energy during braking phases by charging the supercapacitor, whose stored energy is employed by the MGU for successive vehicle acceleration. SCs have been widely recognized in the last two decades as a valid storage system to face up with high peak power in hybrid vehicles [15][14][16][17][18][19][20] allowing the improvement of

management strategies [19][20] [21], anyway a wide literature research revealed that such an electric KERS has never been proposed or studied for ICEV application, above all employing a supercapacitor as single energy storage element. Differently from any other electric KERS proposed for ICEV, the system proposed in this paper allows to use the recovered energy for vehicle acceleration, rather than for electric users supply, thus substantially increasing the amount of recycled energy. Moreover, the low complexity of the system proposed, the reduced volume and weight of the components considered for KERS assembly and their immediate availability on the market, make the solution presented in this paper ready for the introduction in current vehicle production: this could substantially contribute to lower fuel consumption and the related pollutant emissions. Furthermore, differently from Formula 1 application[1], where the sizing of the KERS aims to maximize propulsion power [22], the guidelines followed in the present work aim to optimize vehicle overall cost without causing a marked weight increase, thus allowing the power to be optimally managed during braking and acceleration phases.

The use of Double-Layer-Capacitor (DLC), also known as supercapacitor (SC) or ultracapacitor (UC), as fast and efficient energy storage solution in power application is widely recognized since they offer higher power densities (up to about 3400 W kg^{-1}) with respect to traditional batteries, energy densities from 10 to 20 times higher than common capacitors (up to 30 Wh kg^{-1} [23]) and life cycles up to 10^6: these exceptional capabilities make SC an interesting option when highly dynamic charging or discharging profiles are concerned with high current rates, as for example for vehicle kinetic energy recovery purpose, even in in extreme braking conditions [9][14][24].

However, the major drawbacks of supercapacitors consists in their low volumetric and gravimetric energy density, which makes them not ideal as single energy storage element for electrified vehicles, since large spaces and weights would be involved. For this reason, their high power densities and life cycles have been frequently exploited in conjunction with a second high density energy storage element, in both Electric Vehicles [25][26][27] and Hybrid Electric Vehicles [23][28][29]: in these cases, the SC enhanced the regenerative braking capability of the vehicle by buffering the main storing element (battery or fuel cell) and hence increasing both power and lifetime of the whole energy storage system. The use of a SC as single energy storage element has been proposed only when large spaces and weight were allowed, as for example in the case of electric city rail [30] or hybrid city bus [31], where energy saving of about 40% were obtained. In the present study, instead, the authors aim to evaluate the plausible reduction of fuel consumption, and related CO_2 emissions, that could be achieved by the implementation of the electric KERS proposed in traditional passenger cars endowed of Internal Combustion Engine (ICE), with the aim to improve their sustainability and environmental compatibility. The system proposed in this paper may contribute to the hybridization process of

[1] In this case the energy storage has been realized by the use of lithium-ion battery pack

ICEV, already started with the development of the so called starter-generators system [32], whose growth in power, control complexity and launching ability could further promote the use of supercapacitors as energy storage elements for KERS application.

2 System description

The kinetic energy recovery system proposed in this work is schematically represented in Figure 1 together with the vehicle drivetrain: the supercapacitor (SC), which is the energy storage of the system, is electrically interfaced, through an expressly designed power converter (PC), to the motor generator unit (MGU), which is mechanically connected to the drive shaft via a fixed gear ratio. As clear, the whole system is conceived to be bidirectional, allowing the mechanical power to be converted into electrical power during vehicle braking phases, storing the recovered energy into the SC, and vice versa, using the stored energy to supply the electric motor to produce mechanical power during vehicle acceleration.

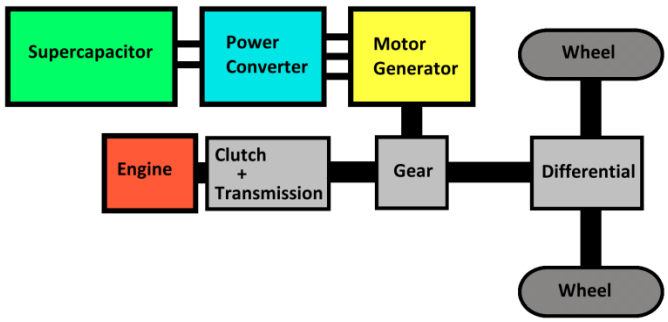

Figure 1 Drivetrain layout of the vehicle with KERS

The most interesting element of the KERS considered in this work is represented by the supercapacitor unit. Supercapacitors (often called also Ultracapacitors) are available on the market with capacitance values up to 3000 F and rated voltage up to 125 V, obtained by means of suitable series-parallel combinations of single SC units [33]. The voltage adaptation between the starter/generator and/or the battery is usually performed by suitable power converters able to guarantee a bidirectional flow of energy with high efficiency [34][25]. When supercapacitors are used to buffer a batteries, an adequate management strategy is needed [35].

As regards the MGU, the author focused on brushless motors due to their prerogative of high efficiency, fast dynamic response, higher power density and longer lifetime with respect to common brushed motor; more in details, three-phase Permanent Magnet Synchronous Motors (PMSM) were selected for their prerogative of delivering high torque with low ripple; as is known, this kind of motor requires a proper controller for the transformation of the DC power into three phases AC power. In the system proposed, the function of the power converter is to manage the power flow between the supercapacitor and the MGU: to this purpose it comprises both a DC/DC converter to fit the SC voltage to the MGU

voltage (and vice versa), and an inverter for the control of the MGU through proper sinusoidal current waveforms. It must be also pointed out that, in this work, the brushless motor is assumed to be current-controlled, i.e. the torque delivered (or received) is controlled by controlling the phase-currents, as described in [36]. In the case here considered, the power converter, whose block diagram is reported in Figure 2, is a buck/boost converter that can be operated in both step-up and step-down configuration, thus adapting the voltage of the SC to the voltage of the MGU [37]; its interleaved topology offers several advantages compared to a traditional single inductor topology: the current can be shared among the inductors thus allowing to reduce conduction losses; when small currents are concerned, a single inductor can be used and the ripple on the current can be reduced by a phase displacement of the pulse width modulation signals, allowing a lower switching frequency to be adopted with advantage in terms of the minimization of switching losses.

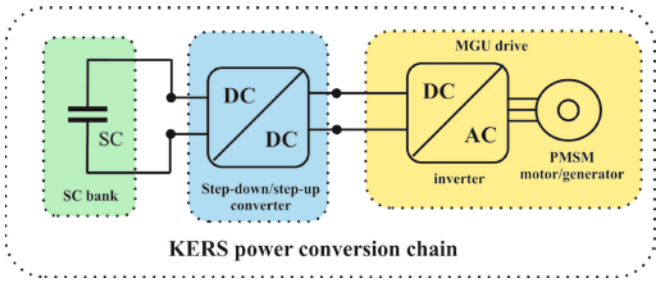

Figure 2 Scheme of the KERS proposed: as shown the power converter comprises both a DC/DC converter and a DC/AC inverter

These conversion topologies have been recently studied to achieve high conversion efficiency assessing a high power density and a reduced cost per kW; a discussion on the optimization of the power converter is beyond of the scope of this paper, but further information can be found in [37][38][39].

The efficiency curve of such power converter [37] is reported in Figure 3 as function of output and input percentage power (due to the high efficiency level, the two curves are almost overlapping): as can be seen, for a power factor in the order of 5%, the efficiency reaches 0.90, while for power factor exceeding 10% of maximum, the efficiency remains at its best value, i.e. 0.93.

The KERS proposed in this work is supposed to operate only during the vehicle transient phases, participating to vehicle acceleration in conjunction with the internal combustion engine, or to vehicle braking in conjunction with the mechanical braking system (e.g. a disc brake system or a drum brake system). More in detail, during a braking phase, the MGU acts as a generator and contributes to reduce the vehicle speed transferring part of the vehicle kinetic energy to the supercapacitor. During a regenerative braking, hence, the power flows from the vehicle wheels to the MGU which charges the supercapacitor: in this case the power converter fits the voltage of the MGU drive to the voltage of the SC and regulates the electric current supplied to the SC according to the power received by the MGU.

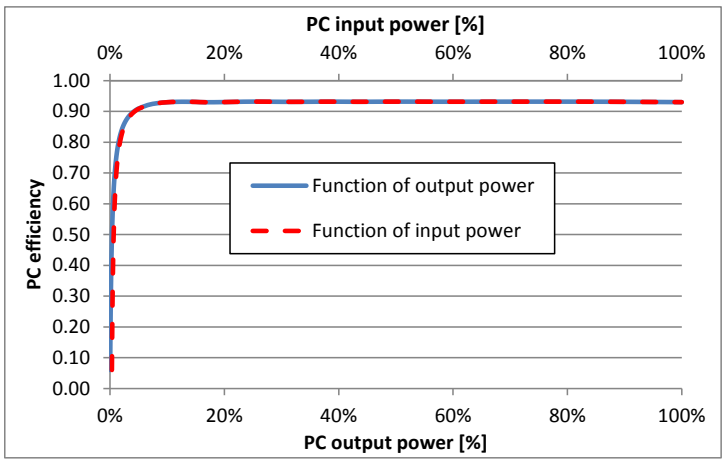

Figure 3 Power converter efficiency as function of both percentage output and input power

During an acceleration phase, instead, the MGU acts as motor and contributes to increase vehicle speed thus reducing the power demand to the internal combustion engine and, as a consequence, its fuel consumption and the related CO_2 emissions. During an acceleration phase, hence, the MGU, supplied by the SC through the power converter, transmits the power to the drive shaft and hence to the wheels: in this case, hence, the power converter adapts the SC voltage to the MGU voltage and control the power transfer from the supercapacitor regulating the electric current supplied to the MGU.

Considering the structure of the KERS proposed (see Figure 1), the power flux involving each element is schematically reported in Figure 4 both for an acceleration and for a braking phase; this diagram helps to identify the magnitude of the power managed by each component of the KERS.

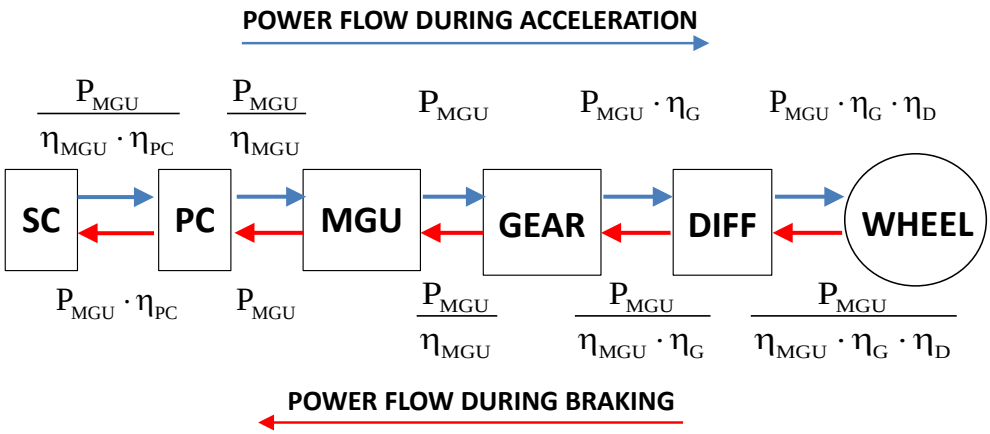

Figure 4 Schematic representation of the KERS power fluxes in both acceleration and braking phase

3 Vehicle dynamics

In general, the elementary equation which takes into account all the forces acting on the longitudinal dynamics of a vehicle is:

$$F_{trac}(t) - F_{br}(t) - \left[F_{aer}(t) + F_{roll}(t) + F_{grav}(t) + F_{dist}(t) \right] = m_v \cdot \frac{d\,v(t)}{dt} = m_v \cdot a(t) \tag{1}$$

where m_v represents the reference mass of the vehicle (which should also comprises the equivalent mass of the rotating parts), *v(t)* and *a(t)* are the vehicle speed and acceleration (functions of time *t*), F_{trac} is the traction force acting on the vehicle as result of the overall motive power, F_{br} is the braking force acting on the vehicle as result of the braking system, F_{aer} is the drag force due to the impact with the air, F_{roll} is the rolling resistance force on the wheels, F_{grav} is the force of gravity acting in the case of a slope and F_{dist} takes into account any other disturbance force of motion, as it could be for example the wind.

The sum of the forces within square brackets constitutes the *road load* F_{road}, which is the resistance to movement and must be overcome by the vehicle to move forward.

$$F_{road}(t) = F_{aer}(t) + F_{roll}(t) + F_{grav}(t) + F_{dist}(t) \tag{2}$$

Hence equation (1) becomes:

$$F_{trac}(t) - F_{br}(t) - F_{road}(t) = m_v \cdot a(t) \tag{3}$$

It is worth to underline that both the resistance to movement F_{road} and the braking force F_{br} always act in the opposite direction of the vehicle speed, thus producing a braking effect; as can be observed in equation (3), in this work these forces have been considered positive, leaving their braking role to the negative sign; on the contrary, the traction force F_{trac} is considered positive when acting in the same direction of vehicle speed. To the purpose of this work, the contributions due to F_{grav} and F_{dist} forces were neglected, since the vehicles were considered to operate in a horizontal plane and without any disturbing forces (as therefore assumed for the execution of standard driving cycles). The aerodynamic resistance F_{aer} can be calculated as:

$$F_{aer}(v) = \frac{1}{2}\delta_a \cdot A_f \cdot c_x(v) \cdot v^2 \tag{4}$$

where δ_a represents the air density (1.225 kg m^{-3} in standard conditions), A_f is the frontal area of the vehicle and c_x is the drag coefficient, which takes into account the air resistance on the vehicle's profile and may vary with vehicle speed. The rolling resistance F_{roll} can be evaluated as:

$$F_{roll}(v) = c_r(v,p) \cdot m_v \cdot g \tag{5}$$

being g the gravitational acceleration and c_r the rolling resistance coefficient, which, besides a marked dependence on the vehicle speed v, should also vary with the tires pressure p. For convenience, however, in this work both the drag coefficient c_x and the rolling resistance coefficient c_r were considered constant.

As a result, multiplying the forces of equation (1) for the vehicle speed $v(t)$, the power balance is obtained:

$$P_{trac}(t) - P_{br}(t) = F_{road}(t) \cdot v(t) + m_v \cdot a(t) \cdot v(t) = P_{road}(t) + P_I(t) \tag{6}$$

where P_{road} ($=F_{road} \cdot v$) is the *road load power*, that is the power necessary to counterbalance the resistance to movement, while P_I ($=m_v \cdot a \cdot v$) is the *inertial power* which instead accounts for the power required by inertia force. As already pointed out, both braking power P_{br} and road load power P_{road} have been considered positive, being their braking function left to the negative sign with respect to traction power.

Equation (6) comprises both traction and braking forces, which in practical situations are not simultaneously present. In a real application, instead, one of the following motion conditions is realized: acceleration, constant speed, braking, coasting.

An acceleration process is characterized by $a(t)>0$ and obviously $P_{br}=0$, hence

$$P_{trac}(t) = m_v \cdot a(t) \cdot v(t) + P_{road}(t) = P_I(t) + P_{road}(t) \tag{7}$$

to perform the acceleration $a(t)>0$, the vehicle requires the sum of the road load power P_{road} (>0) and the inertial power P_I (positive because $a(t)$>0). In other words, due to the braking effect of the resistance to the movement, the energy required to accelerate the vehicle is higher than the variation of the vehicle kinetic energy. In the KERS here proposed, the function of the MGU, during an acceleration phase, is to contribute to the inertial power P_I, exploiting the energy stored in the supercapacitor, thus reducing the power demand to the thermal engine. The road load power P_{road} is instead considered entirely balanced by the thermal engine, which has also to supply the remaining part of the inertial power. It is obvious that, if the MGU completely fulfils the inertial power P_I, the internal combustion engines has to provide only the road load power.

When moving with constant speed, $a(t)=0$ and $P_{br}=0$, hence

$$P_{trac}(t) = P_{road}(t) \tag{8}$$

the inertia force is null and the vehicle requires only the power necessary to counterbalance the resistance to movement. In this condition, the KERS proposed by the authors does not operate.

When coasting, the vehicle proceeds without traction or braking forces ($P_{br}=0$, $P_{trac}=0$), and hence, as shown by equation (3), reduces its speed with a negative acceleration ($a(t)<0$) as a result of the resistance to movement:

$$m_v \cdot a(t) = -F_{road}(t) \tag{9}$$

Or, which is the same,

$$P_I(t) = m_v \cdot a(t) \cdot v(t) = -P_{road}(t) \tag{10}$$

According to the approach followed in this paper, also this condition does not imply any KERS operation.

In a braking phase, instead, the vehicle negative acceleration is the effect of a braking action, hence $P_{br}>0$ (and obviously $P_{trac}=0$); equation (6) hence gives:

$$P_{br}(t) = -m_v \cdot a(t) \cdot v(t) - P_{road}(t) = -P_I(t) - P_{road}(t) \tag{11}$$

which means that, to produce the required negative acceleration $a(t)$, due to the braking effect of the road load, the power that the braking system (which may include the action of the KERS) must absorb is lower than the absolute value of the inertial power. This means that the inertial power cannot be entirely recovered during a regenerative braking, but only the fraction $P_{br}(t)$. In other words, due to the braking effect of the road load, the vehicle kinetic energy cannot be entirely recovered. The function of the MGU during such a braking phase is, hence, to convert and transfer (as much as possible) part of the braking power $P_{br}(t)$ to the supercapacitor, whose stored energy will be employed for successive vehicle accelerations.

4 Mathematical model

The evaluation of the energetic performances obtainable by the system proposed were carried out by means of numerical simulation performed by MATLAB Simulink. In the following sections a detailed description of the equations employed in the numerical simulations is given; for a better understanding, the reader should refer to the power fluxes reported in Figure 4. As already clarified, the KERS proposed in this paper is supposed to operate only during transient phases, reducing the power demand to the thermal engine during vehicle accelerations, and recovering part of the vehicle kinetic energy during the braking phases. It is worth to point out that the calculation always proceeds from the wheel (where the required acceleration or braking power is known) to the supercapacitor: as a results, in the simulation regarding vehicle acceleration, for each element of the KERS proposed, the output power was determined first; in the simulation regarding vehicle braking, instead, the input power of each KERS component was evaluated first.

5.1 Acceleration phases

Focusing on the acceleration phases (i.e. $a(t)>0$), the required vehicle traction power (see equation (7)) can be written as:

$$P_{trac}(t) = P_I(t) + P_{road}(t) = \left[P_{MGU}(t) \cdot \eta_G + P_{eng}(t) \cdot \eta_T \right] \cdot \eta_D \tag{12}$$

being the net contribution of the MGU reduced by the efficiency η_G of the gear adopted (as represented in Figure 1) between the brushless motor and the drive shaft, P_{eng} the power demand to the internal combustion engine, η_T and η_D the efficiency of the main transmission and of the final differential gear respectively. It is worth to remember that the vehicle acceleration condition is $a(t)>0$ ($\Rightarrow P_I(t)>0$) and differs from $P_{trac}(t)>0$, since, due to the road load power $P_{road}(t)$, the traction power $P_{trac}(t)$ is positive also when the vehicle proceeds with constant speed ($a(t)=0$).

As regards the brushless motor, a model was adopted to evaluate the input power $P_{MGU,in}(t)$ of the motor as function of the output power $P_{MGU}(t)$. The power balance of the brushless motor can be represented as:

$$P_{MGU}(t) = T_{MGU}(t) \cdot \omega(t) = P_{MGU,in}(t) - L_{MGU}(t) - I \cdot \alpha(t) \cdot \omega(t) \tag{13}$$

where the output power $P_{MGU}(t)$ is the product between the motor rotation speed $\omega(t)$ and the torque $T_{MGU}(t)$ delivered, $L_{MGU}(t)$ represents the sum of the power losses in the MGU, and the last term represents the inertial power absorbed by the brushless motor (whose rotational inertia is I) subjected to the angular acceleration $\alpha(t)$. On the basis of [40][41] the power losses in the MGU were subdivided into:

1) resistive and power interrupter losses, $L_R(t)$
2) mechanical friction losses, $L_F(t)$
3) windage losses, $L_W(t)$

The first kind of losses mainly depend on the square value of the MGU phase current, and, in turn, on the square value of the current on the DC side of the MGU controller $i_{MGU}(t)$. Indicating with R the proportionality constant, the resistive losses can be expressed as:

$$L_R(t) = R \cdot {i_{MGU}}^2(t) \tag{14}$$

As regards the second kind of losses, according to the usual hypothesis of constant friction torque=T_F, a proportionality with the rotor angular velocity $\omega(t)$ can be assumed, i.e.:

$$L_F(t) = T_F \cdot \omega(t) \tag{15}$$

The third kind of losses, as is generally done, were considered proportional to the cube of the rotor angular velocity by means of the parameter k. Summing up, the power losses in the MGU were modelled as:

$$L_{MGU}(t) = L_R(t) + L_F(t) + L_W(t) = R \cdot {i_{MGU}}^2(t) + T_F \cdot \omega(t) + k \cdot \omega^3(t) \tag{16}$$

The losses parameters R, T_F and k of the MGU can be obtained by means of statistical regression of the experimental data provided by the motor manufacturer. As example, Figure 5 shows the agreement between the measured efficiency and the efficiency computed by the model for the brushless motor Motenergy M1115 [42]:

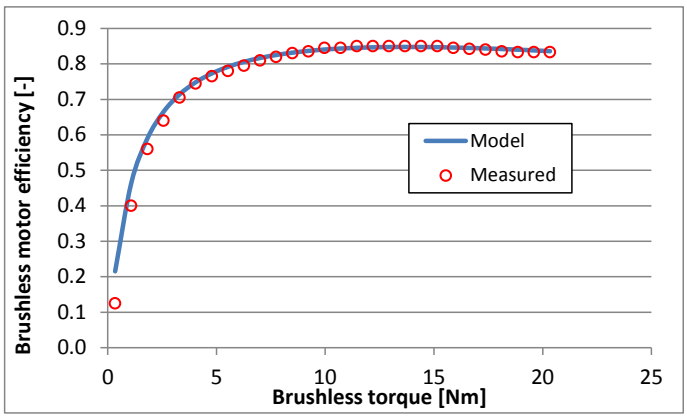

Figure 5 Comparison between measured and simulated brushless motor efficiency

(based on Motenergy ME1115, 69 V_{DC}, 3000 rpm [42])

Once calibrated, the motor model allows to determine the necessary DC input power to the MGU (i.e. $P_{MGU,in}(t)$), which must be provided by the power converter as product of the supply voltage V_{MGU} for the current $i_{MGU}(t)$:

$$P_{PC}(t) = P_{MGU,in}(t) = V_{MGU} \cdot i_{MGU}(t) \tag{17}$$

The power balance of the brushless motor of equation (13) hence becomes:

$$V_{MGU} \cdot i_{MGU}(t) - T_{MGU}(t) \cdot \omega(t) - R \cdot {i_{MGU}}^2(t) - T_F \cdot \omega(t) - k \cdot \omega^3(t) - I \cdot \alpha(t) \cdot \omega(t) = 0 \tag{18}$$

Equation (18) allows to determine the input current to the MGU controller $i_{MGU}(t)$, once the torque to deliver $T_{MGU}(t)$ is known. Three constraints must be however taken into consideration: the first regards the torque delivered by the motor, which is limited by the stall torque $T_{MGU,stall}$, which is a characteristic of the brushless machine. The second constraint regards instead the input current to the MGU controller, which cannot exceeds the maximum allowed value $i_{MGU,max}$, that is another important characteristic of the brushless machine. This further limits the torque that the brushless motor can deliver to the value $T_{MGU,CL}(t)$, which can be obtained by equation (18) once the maximum current $i_{MGU,max}$ is considered, i.e.:

$$T_{MGU,CL}(t) = \frac{V_{MGU} \cdot i_{MGU,\max}(t)}{\omega(t)} - \frac{R \cdot {i_{MGU,\max}}^2(t)}{\omega(t)} - T_F - k \cdot \omega^2(t) - I \cdot \alpha(t) \tag{19}$$

It is worth noting that the current limited torque $T_{MGU,CL}(t)$ depends on the motor rotation speed $\omega(t)$.

Besides the two constraints already mentioned, in the system proposed the power produced by the brushless motor can be further limited by the instantaneous power availability at the supercapacitor $P_{SC,max}(t)$:

$$P_{SC,max}(t) = V_{SC}(t) \cdot i_{PC,max} \tag{20}$$

this power availability depends on the instantaneous working voltage $V_{SC}(t)$ of the supercapacitor, which continuously vary during KERS operation together with the amount of energy stored (and is evaluated through equation (35)), and on the maximum current allowed in the power converter $i_{PC,max}$, which, as will be shown in the paper Part 2, is determined in the KERS sizing procedure to meet its power requirement.

As also shown by Figure 4, the limited output power availability at the supercapacitor may limit the input power to the MGU, whose working current may hence be restricted to:

$$i_{MGU,SL}(t) = \frac{P_{SC,max}(t) \cdot \eta_{PC}(t)}{V_{MGU}} = \frac{V_{SC}(t) \cdot i_{PC,max} \cdot \eta_{PC}(t)}{V_{MGU}} \tag{21}$$

being $\eta_{PC}(t)$ the power converter efficiency, whose value, as shown further on, can be evaluated through equation (31). As a result, the motor output torque is further limited to the value $T_{MGU,SL}(t)$ obtained by equation (18) once the supercapacitor limited current $i_{MGU,SL}(t)$ of equation (21) is considered, i.e.:

$$T_{MGU,SL}(t) = \frac{V_{MGU} \cdot i_{MGU,SL}(t)}{\omega(t)} - \frac{R \cdot {i_{MGU,SL}}^2(t)}{\omega(t)} - T_F - k \cdot \omega^2(t) - I \cdot \alpha(t) \tag{22}$$

As a result, for each rotation speed $\omega(t)$, the maximum torque $T_{MGU,max}(t)$ that the brushless motor can deliver is:

$$T_{MGU,\max}(t) = \min\left(T_{MGU,stall}; T_{MGU,CL}(t); T_{MGU,SL}(t)\right) \tag{23}$$

And the maximum motive power that the brushless motor can deliver is hence:

$$P_{MGU,\max}(t) = T_{MGU,\max}(t) \cdot \omega(t) \tag{24}$$

As clarified by the layout reported in Figure 1, the motor rotation speed $\omega(t)$ depends on the vehicle speed $v(t)$ thorough the vehicle wheel radius R_W, the brushless gear ratio τ_G and the final gear ratio τ_D:

$$\omega(t) = \frac{v(t)}{R_W} \cdot \tau_G \cdot \tau_D \tag{25}$$

Analogously, the motor acceleration $\alpha(t)$ can be evaluated on the basis of the vehicle acceleration $a(t)$:

$$\alpha(t) = \frac{d\omega(t)}{dt} = \frac{a(t)}{R_W} \cdot \tau_G \cdot \tau_D \tag{26}$$

Both wheel radius R_W and differential final gear ratio τ_D depend on the vehicle while the brushless gear ratio τ_G was fixed considering to reach the maximum motor rotation speed at the vehicle speed of 60 km h^{-1} (i.e. the maximum value

within urban driving cycles): it is worth to point out that, according to the system proposed, brushless motor and drive shaft must be disengaged when vehicle speed exceeds 60 km h^{-1}.

As already clarified, in the present paper the motor contribution was restricted to the inertial power $P_I(t)$ necessary for vehicle acceleration; as a consequence, in the simulation performed, the power produced by the MGU was evaluated as:

$$P_{MGU}(t) = \min\left(P_{MGU,\max}(t); \frac{P_I(t)}{\eta_G \cdot \eta_D} \right) \tag{27}$$

where the gear efficiency η_G was assumed 0.97 while the efficiency of the differential η_D was assumed 0.93.

Once determined the power produced by the MGU, the power demand to the internal combustion engine P_{eng} can be deduced from equation (12) as the necessary complement to the total required traction power:

$$P_{eng}(t) = \frac{P_{trac}(t)}{\eta_D \cdot \eta_T} - \frac{P_{MGU}(t)}{\eta_T} \cdot \eta_G = \frac{P_I(t) + P_{road}(t)}{\eta_D \cdot \eta_T} - \frac{P_{MGU}(t)}{\eta_T} \cdot \eta_G \tag{28}$$

In the system proposed, during an acceleration phase, the MGU is supplied by the power converter, whose output power $P_{PC}(t)$, as also shown in Figure 4, constitutes the input power $P_{MGU,in}(t)$ to the MGU and can be determined by equations (17) and (18). The power converter, in turn, is supplied by the supercapacitor, whose output power (as shown in Figure 4) is hence:

$$P_{SC}(t) = \frac{P_{PC}(t)}{\eta_{PC}(t)} \tag{29}$$

being $\eta_{PC}(t)$ the power converter efficiency, evaluated on the basis of the normalized output power ($=P_{PC}(t)/P_{PC,max}$) through equation (30). It is worth to note that the limit of the maximum available power at the supercapacitor $P_{SC,max}(t)$ is already respected through equation (27).

As regards the power converter efficiency $\eta_{PC}(t)$, an analysis performed by means of Curve Expert on the data plotted in Figure 3 allowed to determine its expression as function of the normalized output power $x_{PC}(t)=P_{PC}(t)/P_{PC,max}$:

$$\eta_{PC}(t) = 0.93 - 1.009 \cdot exp(-26.16 \cdot x_{PC}(t)^{0.6128}) \tag{30}$$

or as function of the normalized input power $x_{PC,in}(t)=P_{PC,in}(t)/P_{PC,in,max}$:

$$\eta_{PC}(t) = 0.93 - 280.7 \cdot exp(-15.82 \cdot x_{PC,\text{in}}(t)^{0.1766}) \tag{31}$$

The energy content of the supercapacitor during the (emptying) acceleration process is hence evaluated through integration of the power delivered by the supercapacitor, taking into account its efficiency:

$$E_{SC}(t) = \int_{E_i} dE_{SC} = \int_{E_i} -\frac{P_{SC}(t)}{\eta_{SC}(t)}\, dt \tag{32}$$

where E_i denotes the initial energy content of the SC. The efficiency of the supercapacitor was evaluated by means of its Equivalent Series Resistance (ESR):

$$\eta_{SC}(t) = 1 - \frac{i_{SC}(t) \cdot ESR}{V_{SC}(t)} \tag{33}$$

where $V_{SC}(t)$ and $i_{SC}(t)$ represent the supercapacitor instantaneous working voltage and current. Given the relation between the energy stored in the supercapacitor $E_{SC}(t)$ and its working voltage:

$$E_{SC}(t) = \frac{1}{2} \cdot C \cdot V_{SC}^2(t) \tag{34}$$

the supercapacitor working voltage is evaluated as:

$$V_{SC}(t) = \sqrt{\frac{2 \cdot E_{SC}(t)}{C}} \tag{35}$$

being C the nominal capacitance of the supercapacitor.

The supercapacitor current can be hence evaluated on the basis of the power demand $P_{SC}(t)$ calculated in equation (29):

$$i_{SC}(t) = \frac{P_{SC}(t)}{V_{SC}(t)} \tag{36}$$

The supercapacitor voltage $V_{SC}(t)$ also allows to determine its instantaneous maximum available power $P_{SC,max}(t)$:

$$P_{SC,max}(t) = V_{SC}(t) \cdot i_{PC,max} \tag{37}$$

which represents the maximum power that during an acceleration phase can be delivered by the supercapacitor to the converter, and puts a limit to the supercapacitor rate of discharge (equations (32)) and to the power delivered by the brushless motor (equations (21)).

To account for the necessary minimum working voltage of the supercapacitor $V_{SC,min}$ (supposed to be 20%·of $V_{SC,max}$), the integral of equation (32) is limited in the lower values, i.e. a minimum is imposed to the energy stored in the supercapacitor:

$$E_{SC,\min} = \frac{1}{2} \cdot C \cdot V_{SC,\min}^2 \tag{38}$$

Once reached this minimum energy content in the SC, the system is considered unable to produce power for vehicle acceleration and the MGU output is considered null, thus making all the necessary traction power $P_{trac}(t)$ entirely provided by the thermal engine:

$$P_{MGU}(t) = 0 \text{ if } \begin{cases} a(t) > 0 \\ \text{AND} \\ E_{SC}(t) = E_{SC,\min} \end{cases} \tag{39}$$

5.2 Braking phases

Focusing now on vehicle braking phases, the power $P_{br}(t)>0$ that must be absorbed for vehicle deceleration ($a(t)<0$) is:

$$P_{br}(t) = -m_v \cdot a(t) \cdot v(t) - P_{road}(t) = -P_I(t) - P_{road}(t) \tag{40}$$

Unlike the acceleration case, the authors supposed that in a braking phase the KERS contribution is not restricted, with the aim to convert as much as possible of the braking power. Several constraints however limit also in this case the power that can be recovered by the brushless machine, now acting as a generator, or by the supercapacitor. For the analysis of the brushless generator performances, a model was adopted to evaluate the power received and transferred, taking into account the same losses considered when acting as motor, hence:

$$V_{MGU} \cdot i_{MGU}(t) = T_{MGU}(t) \cdot \omega(t) - i_{MGU}^2(t) \cdot R - T_F \cdot \omega(t) - k \cdot \omega^3(t) - I \cdot \alpha(t) \cdot \omega(t) \tag{41}$$

As is clear, in a braking case, the input is the mechanical power $\omega(t) \cdot T_{MGU}(t)$ received through the drive shaft; after reductions due to resistive and power interrupter losses, to friction losses and to windage losses, the remaining power is converted into DC electrical power $V_{MGU} \cdot i_{MGU}(t)$ by the inverter. It is worth noting that, in a braking phase, the brushless angular acceleration $\alpha(t)$ is negative, and hence the rotor inertial power constitutes a positive power input to the brushless generator. Given hence the mechanical input power, equation (41) allows to determine the current $i_{MGU}(t)$ and hence the related power transmitted by the brushless generator to the power converter.

Once again, several limitations must be adequately taken into account for the calculation of the power received and converted by the KERS: first of all, the maximum torque that the brushless generator can receive cannot exceeds the stall torque $T_{MGU,stall}$. The second limitation is represented by the maximum current $i_{MGU,max}$ allowed on the DC side of the MGU controller, which, further restricts the torque that can be transformed by the brushless generator to the value $T_{MGU,CL}(t)$, evaluated through equation (41) with the use of the maximum allowed current, i.e.:

$$T_{MGU,CL}(t) = \frac{V_{MGU} \cdot i_{MGU,\max}(t)}{\omega(t)} + \frac{R \cdot i_{MGU,\max}{}^2(t)}{\omega(t)} + T_F + k \cdot \omega^2(t) + I \cdot \alpha(t) \tag{42}$$

As also pointed out in the acceleration case, the current limited torque $T_{MGU,CL}(t)$ depends on the motor rotation speed $\omega(t)$.

The third limitation to consider is related to the maximum power that the supercapacitor can receive $P_{SC,max}(t)$ (see equation (54)) which may limit the power transfer between MGU and power converter, and hence, the input torque to the generator; considering that, in the braking case, the current limit imposed by the supercapacitor is:

$$i_{MGU,SL}(t) = \frac{P_{SC,max}(t)}{V_{MGU} \cdot \eta_{PC}(t)} = \frac{V_{SC}(t) \cdot i_{PC,max}}{V_{MGU} \cdot \eta_{PC}(t)} \tag{43}$$

it follows that the torque received by the brushless generator is limited to the value $T_{MGU,SL}(t)$ obtained by equation (41) when the current $i_{MGU,SL}(t)$ is considered:

$$T_{MGU,SL}(t) = \frac{V_{MGU} \cdot i_{MGU,SL}(t)}{\omega(t)} + \frac{R \cdot {i_{MGU,SL}}^2(t)}{\omega(t)} + T_F + k \cdot \omega^2(t) + I \cdot \alpha(t) \tag{44}$$

In equation (43) the power converter efficiency $\eta_{PC}(t)$ is determined through equation (30) on the basis of the normalized output power $x_{PC}=P_{SC,max}(t)/P_{PC,max}$.

As a result, for each rotation speed $\omega(t)$, the maximum torque $T_{MGU,max}(t)$ that the brushless generator can receive during a braking phase is:

$$T_{MGU,\max}(t) = \min\left(T_{MGU,stall}; T_{MGU,CL}(t); T_{MGU,SL}(t)\right) \tag{45}$$

And hence, the maximum power that the brushless machine can receive during a braking phase is:

$$P_{MGU,in,\max}(t) = T_{MGU,\max}(t) \cdot \omega(t) \tag{46}$$

Taking into consideration the efficiency η_G of the brushless gear, the input power to the brushless generator $P_{MGU,in}(t)$ can be computed once the braking power $P_{br}(t)$ is known:

$$P_{MGU,in}(t) = \min\left(P_{MGU,in,\max}(t); P_{br}(t) \cdot \eta_G \cdot \eta_D\right) \tag{47}$$

Once determined the power received by the MGU, the input power $P_{PC,in}(t)$ to the converter is computed through equation (41):

$$P_{PC,\text{in}}(t) = V_{MGU} \cdot i_{MGU}(t) = P_{MGU,in}(t) - {i_{MGU}}^2(t) \cdot R - T_F \cdot \omega(t) - k \cdot \omega^3(t) - I \cdot \alpha(t) \cdot \omega(t) \tag{48}$$

The power input to the supercapacitor is hence evaluated as:

$$P_{SC,in}(t) = P_{PC,\text{in}}(t) \cdot \eta_{PC}(t) = V_{MGU} \cdot i_{MGU}(t) \cdot \eta_{PC}(t) \tag{49}$$

where the efficiency $\eta_{PC}(t)$ of the power converter is computed by means of equation (31) on the basis of its normalized input power $x_{PC,in}=P_{PC,in}(t)/P_{PC,in,max}$.

The energy content of the supercapacitor during a (filling) braking phase is then determined integrating its effective input power, i.e.:

$$E_{SC}(t) = \int_{E_i} dE_{SC} = \int_{E_i} P_{SC,in}(t) \cdot \eta_{SC}(t)\, dt \tag{50}$$

where the SC efficiency is again evaluated as:

$$\eta_{SC}(t) = 1 - \frac{i_{SC}(t) \cdot ESR}{V_{SC}(t)} \tag{51}$$

being $V_{SC}(t)$ the SC working voltage calculated by means of the energy content $E_{SC}(t)$ and of the capacitance C of the supercapacitor:

$$V_{SC}(t) = \sqrt{\frac{2 \cdot E_{SC}(t)}{C}} \tag{52}$$

while the current $i_{SC}(t)$ is evaluated on the basis of the power input to the supercapacitor (equation (49)):

$$i_{SC}(t) = \frac{P_{SC,in}(t)}{V_{SC}(t)} \tag{53}$$

The supercapacitor voltage $V_{SC}(t)$ also allows to determine its instantaneous maximum input power $P_{SC,\,max}(t)$:

$$P_{SC,max}(t) = V_{SC}(t) \cdot i_{PC,max} \tag{54}$$

which, as shown in equation (47), limits the power that can be transferred during a braking phase, and hence the supercapacitor rate of charge (equations (50)).

As obvious, the integration in equation (50) was limited to the maximum energy storable in the supercapacitor, which is:

$$E_{SC,\max} = \frac{1}{2} \cdot C \cdot V_{SC,\max}^2 \tag{55}$$

Once reached this upper limit, the KERS is considered unable to receive further power, the input power to the MGU is considered null, thus making all the necessary braking power $P_{br}(t)$ entirely provided by the mechanical braking system of the vehicle:

$$P_{MGU,in}(t) = 0 \;\text{ if }\; \begin{cases} P_{br}(t) > 0 \\ \text{AND} \\ E_{SC}(t) = E_{SC,\max} \end{cases} \tag{56}$$

5 Conclusions

In this first part of a two-papers work the authors propose an electric KERS for internal combustion engine vehicle. The system was conceived to recover the vehicle kinetic energy during braking phases, to be re-used in successive vehicle acceleration phases, so as to reduce the power demand to the internal combustion engine, and, as a consequence, the related fuel consumption and pollutant emissions. An accurate description of the system proposed is given in this first paper, together with a detailed mathematical model realized by the authors with the aim to evaluate the probable energetics and economics performances of the KERS by means of numerical simulations. For each component of the

KERS, the model evaluates its real efficiency during operation, taking into account the limitations introduced in terms of both storable energy or transferrable power. The model was then employed for numerical simulation performed with Matlab Simulink, whose results are presented in the paper Part 2.

6 References

[1] Iodice, P., Senatore, A., “Experimental-analytical investigation to estimate an emission inventory from road transport sector”, (2014) IAENG Transactions on Engineering Sciences - Special Issue of the International MultiConference of Engineers and Computer Scientists, IMECS 2013 and World Congress on Engineering, WCE 2013, pp. 141-149.

[2] Iodice, P., Senatore, A., Langella, G., Amoresano, A., "Advantages of ethanol–gasoline blends as fuel substitute for last generation Si engines", (2017) Environmental Progress and Sustainable Energy, 36 (4), pp. 1173-1179, DOI: 10.1002/ep.12545

[3] Pipitone, E., Genchi, G., Experimental determination of liquefied petroleum gas-gasoline mixtures knock resistance, (2014) Journal of Engineering for Gas Turbines and Power, 136 (12), art. no. 121502, DOI: 10.1115/1.4027831

[4] M. Cammalleri, D. Rotella, Functional design of power-split CVTs: an uncoupled hierarchical optimized model, Mech. Mach. Theory 116 (2017) 294–309.

[5] D. Rotella, M. Cammalleri, Direct analysis of power-split CVTs: A unified method, Mech. Mach. Theory 121 (2018) 116–127

[6] Zhou, Y., Ravey, A., & Péra, M. C. (2019). A survey on driving prediction techniques for predictive energy management of plug-in hybrid electric vehicles. Journal of Power Sources, 412, 480-495, DOI: 10.1016/j.jpowsour.2018.11.085.

[7] Zhou, W., Yang, L., Cai, Y., & Ying, T. (2018). Dynamic programming for new energy vehicles based on their work modes Part II: Fuel cell electric vehicles. Journal of Power Sources, 407, 92-104, DOI: 10.1016/j.jpowsour.2018.10.048

[8] Thounthong, P., Raël, S., & Davat, B. (2006). Control strategy of fuel cell/supercapacitors hybrid power sources for electric vehicle. Journal of Power Sources, 158(1), 806-814, DOI: 10.1016/j.jpowsour.2005.09.014

[9] Faggioli, E., Rena, P., Danel, V., Andrieu, X., Mallant, R., & Kahlen, H. (1999). Supercapacitors for the energy management of electric vehicles. Journal of Power Sources, 84(2), 261-269, DOI: 10.1016/S0378-7753(99)00326-2

[10] Sovran, G. and Blaser, D., "Quantifying the Potential Impacts of Regenerative Braking on a Vehicle's Tractive-Fuel Consumption for the U.S., European, and Japanese Driving Schedules," SAE Technical Paper 2006-01-0664, 2006, https://doi.org/10.4271/2006-01-0664

[11] Gabriel-Buenaventura, A., Azzopardi, B., Energy recovery systems for retrofitting in internal combustion engine vehicles: A review of techniques, (2015), Renewable and Sustainable Energy Reviews, 41, pp. 955-964, DOI: 10.1016/j.rser.2014.08.083

[12] Thomas M., Nishanth D., Flywheel based kinetic energy recovery systems (KERS) integrated in vehicles, International Journal of Engineering Science and Technology (IJEST), 2013, Vol. 5, No.09, pp. 1694-1699, ISSN : 0975-5462

[13] Dimitrova, Z., Maréchal, F., Gasoline hybrid pneumatic engine for efficient vehicle powertrain hybridization, (2015), Applied Energy, 151, pp. 168-177, DOI: 10.1016/j.apenergy.2015.03.057

[14] http://www.bmw.com.af/com/en/insights/technology/efficientdynamics/phase_1/measures_brake_energy_regeneration.html

[15] Kouchachvili, L., Yaïci, W., & Entchev, E. (2018). Hybrid battery/supercapacitor energy storage system for the electric vehicles. Journal of Power Sources, 374, 237-248, DOI: 10.1016/j.jpowsour.2017.11.040

[16] Solero, L., Lidozzi, A., Serrao, V., Martellucci, L., & Rossi, E. (2011). Ultracapacitors for fuel saving in small size hybrid vehicles. Journal of Power Sources, 196(1), 587-595, DOI: 10.1016/j.jpowsour.2009.07.041

[17] Burke, A., & Miller, M. (2011). The power capability of ultracapacitors and lithium batteries for electric and hybrid vehicle applications. Journal of Power Sources, 196(1), 514-522, DOI: 10.1016/j.jpowsour.2010.06.092

[18] Al Sakka, M., Gualous, H., Van Mierlo, J., & Culcu, H. (2009). Thermal modeling and heat management of supercapacitor modules for vehicle applications. Journal of Power Sources, 194(2), 581-587, DOI: 10.1016/j.jpowsour.2009.06.038

[19] Li, H., Ravey, A., N'Diaye, A., & Djerdir, A. (2018). A novel equivalent consumption minimization strategy for hybrid electric vehicle powered by fuel cell, battery and supercapacitor. Journal of Power Sources, 395, 262-270, DOI: 10.1016/j.jpowsour.2018.05.078

[20] Carignano, M. G., Costa-Castelló, R., Roda, V., Nigro, N. M., Junco, S., & Feroldi, D. (2017). Energy management strategy for fuel cell-supercapacitor hybrid vehicles based on prediction of energy demand. Journal of Power Sources, 360, 419-433, DOI: 10.1016/j.jpowsour.2017.06.016

[21] Thounthong, P., Rael, S., & Davat, B. (2009). Energy management of fuel cell/battery/supercapacitor hybrid power source for vehicle applications. Journal of Power Sources, 193(1), 376-385, DOI: 10.1016/j.jpowsour.2008.12.120

[22] Upendra K. , Grauers A. , (2015) “Analysis of 2014 Formula one hybrid powertrain”, Chalmers University of Technology, Department of Signals and Systems, http://emobilitycentre.se/en/category/fordonsanalys/

[23] E. Chemali, M. Preindl, P. Malysz and A. Emadi, "Electrochemical and Electrostatic Energy Storage and Management Systems for Electric Drive Vehicles: State-of-the-Art Review and Future Trends," in IEEE Journal of Emerging and Selected Topics in Power Electronics, vol. 4, no. 3, pp. 1117-1134, Sept. 2016, doi: 10.1109/JESTPE.2016.2566583

[24] K. Itani, A. De Bernardinis, Z. Khatir, A. Jammal and M. Oueidat, "Regenerative Braking Modeling, Control, and Simulation of a Hybrid Energy Storage System for an Electric Vehicle in Extreme Conditions," in IEEE Transactions on Transportation Electrification, vol. 2, no. 4, pp. 465-479, Dec. 2016, doi: 10.1109/TTE.2016.2608763

[25] F. Akar, Y. Tavlasoglu, E. Ugur, B. Vural and I. Aksoy, "A Bidirectional Nonisolated Multi-Input DC–DC Converter for Hybrid Energy Storage Systems in Electric Vehicles," in IEEE Transactions on Vehicular Technology, vol. 65, no. 10, pp. 7944-7955, Oct. 2016, doi: 10.1109/TVT.2015.2500683

[26] Zou, Z., Cao, J., Cao, B., Chen, W., Evaluation strategy of regenerative braking energy for supercapacitor vehicle, (2015) ISA Transactions, 55, pp. 234-240, DOI: 10.1016/j.isatra.2014.09.011

[27] Ziyou Song, Heath Hofmann, Jianqiu Li, Jun Hou, Xuebing Han, Minggao Ouyang, Energy management strategies comparison for electric vehicles with hybrid energy storage system, Applied Energy, Volume 134, 2014, Pages 321-331, ISSN 0306-2619, http://dx.doi.org/10.1016/j.apenergy.2014.08.035.

[28] Rambaldi, L., Bocci, E., Orecchini, F., Preliminary experimental evaluation of a four wheel motors, batteries plus ultracapacitors and series hybrid powertrain, (2011) Applied Energy, 88 (2), pp. 442-448, DOI: 10.1016/j.apenergy.2010.08.008

[29] Feroldi, D., Carignano, M., Sizing for fuel cell/supercapacitor hybrid vehicles based on stochastic driving cycles, (2016) Applied Energy, 183, pp. 645-658. , DOI: 10.1016/j.apenergy.2016.09.008

[30] Jisheng Hu, Yukun Zhao and Xiaojing Liu, "The design of regeneration braking system in light rail vehicle using energy-storage Ultra-capacitor," 2008 IEEE Vehicle Power and Propulsion Conference, Harbin, 2008, pp. 1-5, doi: 10.1109/VPPC.2008.4677708.

[31] Ouyang, M., Zhang, W., Wang, E., Yang, F., Li, J., Li, Z., Yu, P., Ye, X., Performance analysis of a novel coaxial power-split hybrid powertrain using a CNG engine and supercapacitors, (2015) Applied Energy, 157, pp. 595-606, DOI: 10.1016/j.apenergy.2014.12.086

[32] B. Lequesne, "Automotive Electrification: The Nonhybrid Story," in IEEE Transactions on Transportation Electrification, vol. 1, no. 1, pp. 40-53, June 2015, doi: 10.1109/TTE.2015.2426573

[33] Vitale G., (2016) “Supercapacitor Modelling by Lagrange’s Equations”, International Conference on Modern Electrical Power Engineering, (ICMEPE-2016), las Palmas de Gran Canaria 6 - 8 of July.

[34] J. Kloetzl and D. Gerling, "An interleaved buck-boost-converter combined with a supercapacitor-storage for the stabilization of automotive power nets," 2011 IEEE Vehicle Power and Propulsion Conference, Chicago, IL, 2011, pp. 1-6, doi: 10.1109/VPPC.2011.6042982

[35] K. M. So, Y. S. Wong, G. S. Hong and W. F. Lu, "An improved energy management strategy for a Battery/Ultracapacitor Hybrid Energy Storage System in Electric Vehicles," 2016 IEEE Transportation Electrification Conference and Expo (ITEC), Dearborn, MI, 2016, pp. 1-6, doi: 10.1109/ITEC.2016.7520186.

[36] Dixon, J.W., Leal, I.A., (2002), “Current control strategy for brushless dc motors based on a common DC signal”, IEEE Transactions on Power Electronics, 17 (2), pp. 232-240, DOI: 10.1109/63.988834

[37] Vitale G., Pipitone E., (2019), “A Six Legs Buck-boost Interleaved Converter for KERS Application”, submitted for publication to World Electric Vehicle Journal, currently available for consultation at http://emilianopipitone.altervista.org/publication_list.htm

[38] Vitale G., (2016) “Energy saving by power electronics: towards a new concept of renewable source”, Invited paper - Plenary Session, International Conference on Renewable Energies and Power Quality (ICREPQ’16) Madrid (Spain), 4th to 6th May.

[39] C. Gammeter, F. Krismer and J. W. Kolar, "Comprehensive Conceptualization, Design, and Experimental Verification of a Weight-Optimized All-SiC 2 kV/700 V DAB for an Airborne Wind Turbine," in IEEE Journal of Emerging and Selected Topics in Power Electronics, vol. 4, no. 2, pp. 638-656, June 2016, doi: 10.1109/JESTPE.2015.2459378

[40] P. Andrada, M.Torrent, J.I.Perat, B. Blanqué, 2004, "Power Losses in Outside-Spin Brushless D.C. Motors", Renewable Energy & Power Quality Journal, Vol.1, No.2, doi.org/10.24084/repqj02.320

[41] James Kuria, Pyung Hwang, 2011, "Modeling Power Losses in Electric Vehicle BLDC Motor", Journal of Energy Technologies and Policy, ISSN 2224-3232, Vol.1, No.4

[42] http://www.motenergy.com/me1115motor.html

7 Symbols and abbreviations

a, $a(t)$	vehicle acceleration, as function of time t
A_f	frontal area of the vehicle
C	Capacitance
CNG	Compressed natural gas
CVT	Continuous variable transmission
c_r	rolling resistance coefficient
c_x	drag coefficient of the vehicle
E_{SC}	energy stored in the supercapacitor
$E_{SC,max}$	maximum storable energy in the supercapacitor
$E_{SC,min}$	minimum allowed energy content of the supercapacitor
ECE-15	European urban driving cycle
ESR	Equivalent series resistance of the supercapacitor
F_{aer}	vehicle aerodynamic resistance
F_{br}	braking force acting on the vehicle
F_{dist}	external disturbance force acting on the vehicle
F_{grav}	force of gravity acting on the vehicle in the case of a slope
F_{road}	Road load (vehicle resistance to the movement)
F_{roll}	vehicle rolling resistance
F_{trac}	traction force acting on the vehicle
I	MGU rotor inertia
i_{MGU}	Current on the DC side of the MGU controller
$i_{MGU, max}$	Maximum allowed current on the DC side of the MGU controller
$i_{MGU, SL}$	MGU current limit imposed by the maximum power output of the supercapacitor
$i_{PC,max}$	Maximum allowed current in the power converter
i_{SC}	Current in the supercapacitor
ICE	Internal combustion engine
ICEV	Internal combustion engine vehicle

k	windage losses constant of the MGU
$KERS$	Kinetic Energy Recovery System
L_F	mechanical friction losses of the MGU
L_{MGU}	MGU power losses
L_R	resistive and power interrupter losses of the MGU
L_W	windage losses of the MGU
m_v	vehicle mass
MGU	Motor Generator Unit
$n_{MGU,\ max}$	Maximum rotation speed of the MGU
p	tires pressure
P_{br}	braking power
p_E	Loss of energy Boolean variable
P_{eng}	power output from the internal combustion engine
P_I	Inertial power
p_L	Loss of power Boolean variable
P_{MGU}	power output from the MGU
$P_{MGU,max}$	maximum power output from the MGU
$P_{MGU,in}$	power input to the MGU
$P_{MGU,in,max}$	maximum power input to the MGU
P_{PC}	power output from the power converter
$P_{PC,max}$	maximum power output from the power converter
$P_{PC,in}$	power input to the power converter
$P_{PC,in,max}$	maximum power input to the power converter
P_{road}	road load power
P_{SC}	power output from the supercapacitor
$P_{SC,in}$	power input to the supercapacitor
$P_{SC,max}$	maximum power output from the supercapacitor
P_{trac}	traction power acting on the vehicle
PC	power converter
$PMSM$	permanent magnet synchronous motor
R	the resistive losses constant of the MGU

$\boldsymbol{RMS}$	Root mean square value
$\boldsymbol{R_W}$	vehicle wheel radius
$\boldsymbol{SC}$	Supercapacitor
$\boldsymbol{t}$	Time
$\boldsymbol{T_F}$	constant friction torque of the MGU
$\boldsymbol{T_{MGU}}$	torque delivered by the MGU
$\boldsymbol{T_{MGU,\,CL}}$	MGU torque limit imposed by the maximum allowed current $i_{MGU,max}$
$\boldsymbol{T_{MGU,\,SL}}$	MGU torque limit imposed by the maximum power output of the supercapacitor
$\boldsymbol{T_{MGU,\,stall}}$	peak stall torque of the MGU
$\boldsymbol{v,\ v(t)}$	vehicle speed, as function of time t
$\boldsymbol{V_{MGU}}$	voltage on the DC side of the MGU controller
$\boldsymbol{V_{MGU,\,max}}$	maximum allowed voltage on the DC side of the MGU controller
$\boldsymbol{V_{SC}}$	instantaneous working voltage of the supercapacitor
$\boldsymbol{V_{SC,\,max}}$	maximum allowed voltage of the supercapacitor
$\boldsymbol{x}_{PC}$	normalized output power from the power converter
$\boldsymbol{x}_{PC,in}$	normalized input power to the power converter